Proceedings of 2013 SEM Annual Conference and Exposition on Experimental and Applied Mechanics,
June 3-5, 2013, Lombard, IL, 2013

Dynamic Buckling of Submerged Tubes due to Impulsive External Pressure

Neal P. Bitter, California Institute of Technology
1200 E. California Blvd, Pasadena, CA 91125, USA
E-mail: nbitter@caltech.edu

Joseph E. Shepherd, Professor, California Institute of Technology
1200 E. California Blvd, Pasadena, CA 91125, USA
E-mail: joseph.e.shepherd@caltech.edu

ABSTRACT
An annular geometry is used to experimentally study fluid-structure interaction and dynamic buckling of tubes submerged in water and subjected to axially-propagating pressure waves. Wave propagation, vibration, and buckling of the specimen tubes are characterized using pressure and strain measurements. Emphasis is placed on pressures near or slightly exceeding the buckling threshold, where buckling deformation is excited but remains elastic or only slightly plastic due to the short duration of the pressure pulse. Measured wave speeds and non-axisymmetric vibration frequencies are in good agreement with predictions from simple fluid-structure interaction models. Near the buckling threshold, the amplitude of non-axisymmetric deformation is observed to grow rapidly with small increases in pressure until plastic deformation occurs, which results in a substantial loss of strength of the tube. Systematic mode 2 variations in wall thickness are found to control the buckle orientation, since the major axis of mode 2 buckles is always aligned with the location where the tube wall is thinnest.

Keywords: Dynamic buckling, fluid-structure interaction, buckling threshold, imperfect structures, impulsive loads

Introduction

Submerged cylindrical tubes and pipes are routinely used in a variety of marine applications, such as submersible vehicles, drilling and mining equipment, and trans-ocean pipelines and communication networks. In addition to withstanding the hydrostatic pressure of the target environment, many of these submerged structures must also survive dynamic loads, such as those due to underwater blasts. In this paper, a unique annular geometry and projectile impact facility is used to study the buckling of cylindrical tubes under these types of load conditions.

Dynamic buckling of tubes subjected to external blast waves has been studied by a number of researchers. Lindberg investigated buckling of very thin shells with ratios of radius to thickness of about $a/h = 480$ and found that the response was governed by elastic effects alone [1]. For much thicker tubes with a/h = 10-30, Abrahamson et al. found that the buckle development is dominated by the effects of plasticity [2]. For intermediate cases, the behavior is more complex since both elastic and plastic effects are important [3]. In addition to studying various tube geometries, experiments have also been conducted under a wide range of load conditions, ranging from impulsive to quasi-static [4, 5, 6, 7].

A significant challenge in the experiments cited above was making comparisons between experimental measurements and theoretical predictions. In most of the experiments, the response of the tube was analyzed only by post-collapse examination, so the behavior during the initial stages of buckling could not be evaluated. In a few cases [4, 8], strain measurements were taken as the tube buckled, but only limited data was reported. In the present experiments, tubes are loaded using shock waves in water rather than blast waves in air, which facilitates dynamic strain measurement during the buckling of the tube. These experiments also explore the effects of fluid-structure interaction that are introduced by the presence of a dense fluid surrounding the tube.

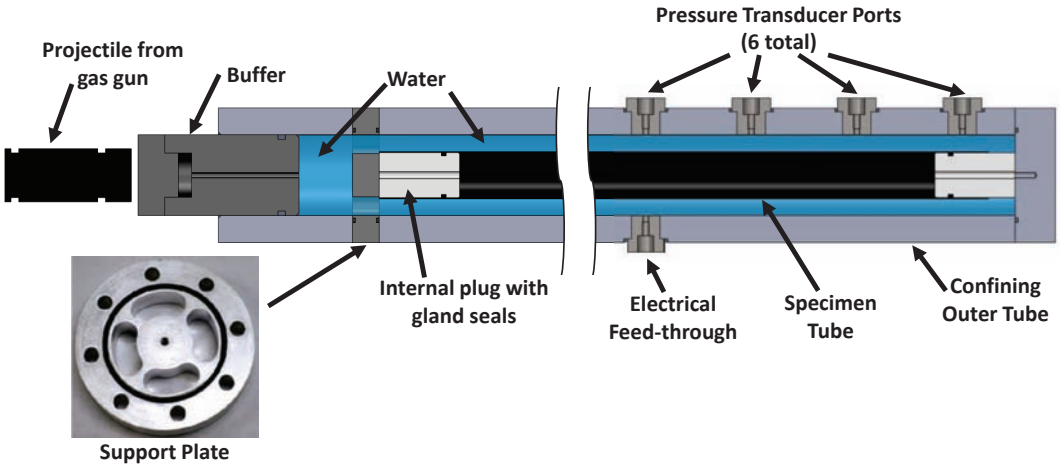

Fig. 1 Diagram of experimental apparatus. Inset photograph shows a support plate used to prevent axial loading of the specimen tube.

Experimental Setup

In this paper, buckling of tubes is studied using shock waves in an annulus of water surrounding a specimen tube. The apparatus, shown in Fig. 1, consists of a thin-walled specimen tube mounted concentrically inside of a larger, thick-walled cylindrical vessel. The outer vessel is made from 4140 high strength steel and has an inner radius of 38.1 mm, wall thickness of 25.4 mm, and length 0.97 m. Specimen tubes are mounted concentrically inside of this vessel, and the ends of the specimen are supported and sealed using internal plugs with gland seals. These plugs restrict inward radial motion of the specimen tube at its ends, but they do not constrain axial motion. However when the tube compresses under external pressure, friction between the inside of the specimen tube and these plugs may constrain axial motion as well. The upper plug, located on the left side of Fig. 1, is mounted to a support plate which prevents axial loads on the specimen tube. As shown in the inset photograph, this support plate features four holes which allow pressure waves to pass through with minimal obstruction.

The annular gap between the specimen tube and the outer cylinder is filled with distilled water, and a buffer is inserted into the top of the fixture. A vertically oriented gas gun then fires a projectile into the buffer, which produces a stress wave in the buffer that is then transmitted into the water. The gas gun, described in more detail in ref. [9], consists of a vertically oriented barrel (50 mm inner diameter) connected to a compressed air reservoir. A 1.5 kg, 120 mm long steel projectile with a flat front is used and is sealed against the gas gun barrel by a pair of o-rings. Prior to the shot, the gas gun's chamber behind the projectile is evacuated so that the projectile is held in place by the vacuum. The compressed air reservoir is then charged to the desired initial pressure, typically between 140 and 350 kPa. Finally, remotely operated valves close the vacuum line and connect the air reservoir to the chamber, launching the projectile down the tube. Typical projectile speeds are between 6 and 30 m/s.

As the projectile emerges from the gas gun barrel, it impacts the buffer shown in Fig. 1. The buffer is 76 mm in diameter and 127 mm long, made from either 6061-T6 aluminum or 304 stainless steel, and capped with a steel striker plate to prevent damage during the projectile impact. During impact, a compressive stress wave is produced in the buffer which is then transmitted into the water. This shock wave then passes through the holes in the support plate and travels axially along the outside of the specimen tube. The pressure pulse consists of sharp shock wave followed by an approximately exponential decay of pressure, and the time constant of this decay is governed by the wave mechanics in the projectile and buffer. Thus by changing the lengths and materials of these two components, the duration of the pressure pulse can be adjusted. Unless stated otherwise, the results in this paper were obtained using a 6061-T6 aluminum buffer.

The pressure load applied to the specimen tube is measured using a row of six pressure transducers (PCB model 113A23) which have a response time less than 1 μs and a resonant frequency greater than 500 kHz. These transducers are positioned in increments of 150 mm along the thick-walled outer tube and are mounted flush with the inner surface of that tube. Since the annulus of water between the specimen tube and the outer cylinder is only 15-20 mm in width, the radial transit time of pressure waves is 10-15 μs, which is much shorter than the other timescales involved in the response of the tube and the motion of the pressure wave. As a result, the pressure measured by the transducers is expected to be very close to the actual pressure at the surface of the specimen tube.

The response of the specimen tube is measured using bonded strain gauges which are coated with a compliant sealant (Vishay

PG, M-Coat D) to prevent degradation of the adhesive and electrical interference due to the surrounding water. Strain measurements are amplified using a Vishay 2310B signal conditioner operated in wide-band mode, which corresponds to a -3 dB cutoff frequency of 250 kHz. All pressure and strain signals are simultaneously digitized at 1 MHz.

Specimen Tubes

Specimen tubes were made from either 6061-T6 aluminum or 304 stainless steel and were 0.91 m long. The dimensions of the tubes discussed in this paper are listed in Table 1. A key parameter affecting the buckling behavior is the ratio a/h, which falls in the range of 17-25 in these experiments.

Table 1 Properties of specimen tubes. Static buckling threshold p_{static} calculated using Eq. 1.

Tube Number	Material	Mean Radius a [mm]	Wall Thickness h [mm]	a/h	p_{static} [MPa]
30	6061-T6 Alum.	15.4	0.89	17.4	3.67
32	6061-T6 Alum.	21.8	0.89	24.5	1.31
34	6061-T6 Alum.	21.8	0.89	24.5	1.31
36	304 Stainless	15.4	0.89	17.4	10.0
42	6061-T6 Alum.	15.4	0.89	17.4	3.67
43	6061-T6 Alum.	15.4	0.89	17.4	3.67
46	6061-T6 Alum.	21.8	1.24	17.5	3.61
47	6061-T6 Alum.	21.8	0.89	24.5	1.31
50	6061-T6 Alum.	21.8	0.89	24.5	1.31
52	6061-T6 Alum.	21.8	0.89	24.5	1.31
54	304 Stainless	21.6	1.17	18.5	8.16

Wall Thickness Variations

It is well-known that tube imperfections play a critical role in determining the static buckling limit [10, 11] and are expected to play a similarly important role in dynamic buckling. One important type of imperfection is the shape imperfection, which consists of an initial non-circularity of the tube in the absence of applied loads. A second type of imperfection is wall thickness variation, in which the wall thickness varies around the circumference of the tube.

In an effort quantify these imperfections, the wall thickness of each tube was measured at various points around the circumference using a round-tipped micrometer. Aluminum tubes, which were manufactured seamlessly by extrusion, featured systematic variations in wall thickness around the circumference. The size of these variations was typically 2-4% of the mean wall thickness for 6061-T6 aluminum, though for other alloys variations as high as 10% were observed. A sampling of these measurements demonstrating the sinusoidal variation of wall thickness is provided in Fig. 2. These systematic variations appear to be uniform, or at least slowly varying, along the axis of the tube since the wall thickness profile is similar at both ends. No attempt was made to measure the shape imperfection of the tubes, i.e., the deviation from circularity. However, the wall thickness variation appears to the most important imperfection since, without exception, tubes that buckled in a mode 2 shape formed buckles that were aligned with the points of minimum and maximum wall thickness.

The steel tubes selected for this experiment were of welded construction, and systematic wall thickness variations were not observed. Instead, the wall thickness was close to uniform around the circumference except in the vicinity of the weld, where a localized region of lesser wall thickness was measured. Although for some tubes the buckles were exactly aligned with the welds, this was not exclusively the case.

Results

Depending on the amplitude and impulse of the pressure wave, the response of the specimen tubes can be divided into several regimes. For low enough pressures, the tube remains axisymmetric during the entire response. At moderate pressures, elastic buckles begin to develop, but if the impulse of the load is small these buckles do not grow large enough to induce plastic deformation. As the pressure or impulse is increased further, however, plastic deformation will eventually occur. Finally, for very large pressures the tube collapses catastrophically during a single load event.

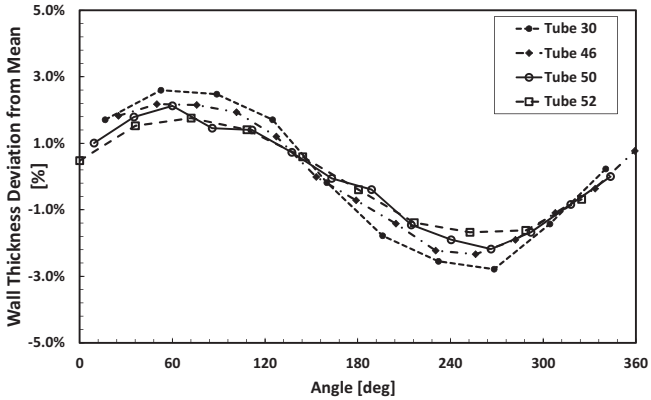

Fig. 2 Variations in wall thickness around the circumference of four specimen tubes. Variations are reported as percentages of the mean wall thickness.

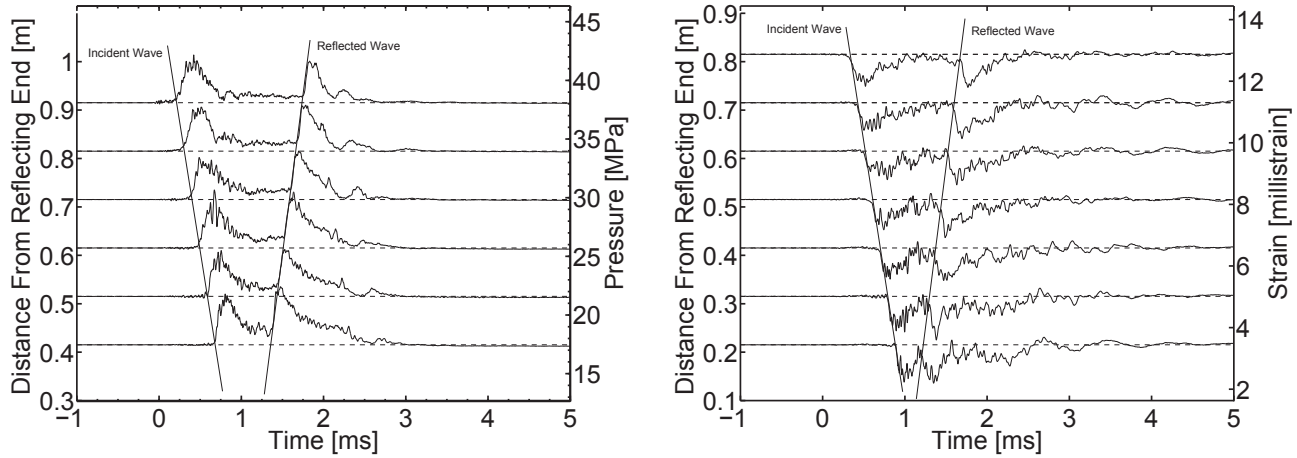

Fig. 3 Pressure (a) and strain (b) histories for Tube 42. The peak pressure is 5.0 MPa and the static buckling pressure is 3.67 MPa.

Linear Elastic Regime

For pressure waves of small amplitude or low impulse, the tube's response is elastic and primarily axisymmetric. Examples of pressure and strain traces in this regime are plotted in Fig. 3. Figure 3a shows that the pressure wave has the form of an exponential that travels along the tube with approximately fixed speed and shape. The pressure wave then reflects off of the bottom end of the test fixture and traverses the specimen tube once more.

The classical static buckling pressure for a long tube is given by [12]:

$$p_{static} = \frac{Eh^3}{4a^3(1-\nu^2)} \tag{1}$$

For the tube corresponding to Fig. 3, the static buckling pressure is only about 3.7 MPa while the peak measured pressure is about 5 MPa. As will be demonstrated in subsequent sections, buckling does not occur because non-axisymmetric deformation grows too slowly to become significant during the short duration of the pressure load.

Figure 3b shows the corresponding hoop strain traces at seven locations along the tube. The strain traces appear to mirror the pressure traces, with the exception of high frequency vibrations that are more prominent in the strain measurements than in the pressure traces. For these low pressures, the response is analogous to that of a waterhammer event occurring on the inside of

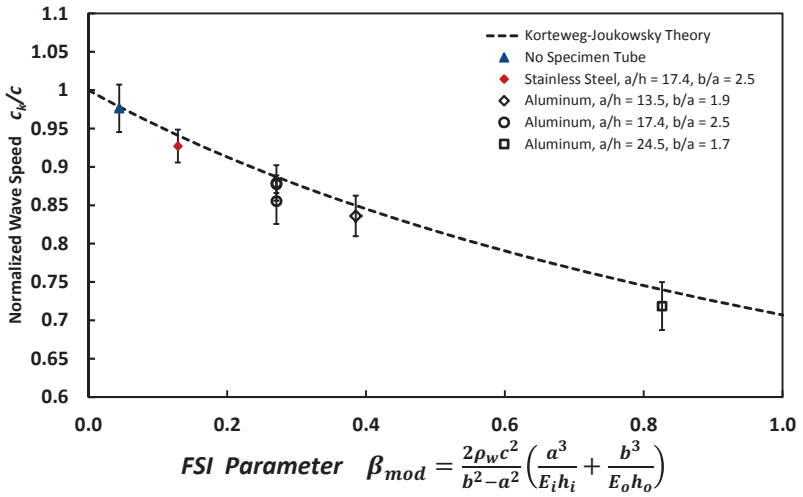

Fig. 4 Comparison of measured wave speeds with the predictions of the modified Korteweg-Joukowsky theory for several tube materials and sizes

a tube. Inaba and Shepherd studied this scenario using a very similar projectile impact facility [9] and recorded pressure and strain traces that look very similar to those of Fig. 3.

The similarity between the present results and the response of a tube during a waterhammer-type event suggests that for low pressures in which buckling does not occur, the response may be predicted using suitably adapted waterhammer models. One of the simplest waterhammer models was first proposed by Korteweg [13] and later applied to waterhammer experiments by Joukowsky [14]. Commonly termed the Korteweg-Joukowsky model, this theory is based on the assumptions that radial inertia of the tube and fluid as well as axial bending of the tube are small [15]. Under these approximations, the speed c_{KJ} of the coupled fluid-solid wave is given by:

$$c_{KJ} = \frac{c}{\sqrt{1+\beta}} \tag{2}$$

where

$$\beta = \rho_w c^2 \frac{2a}{Eh} \tag{3}$$

Here c and ρ_w are the acoustic speed and density of the water, E is the elastic modulus of the tube, and a and h are the mean radius and wall thickness. The parameter β describes the extent of the fluid-solid coupling, which increases as β increases and hence reduces the velocity of the wave motion. This model can be adapted for the current experimental setup in which pressure waves propagate in the annular space between two flexible tubes. The speed of these pressure waves is still in the form of (2), but the fluid-structure interaction parameter β must be replaced with a modified parameter given by:

$$\beta_{mod} = \frac{2\rho_w c^2}{b^2 - a^2}\left(\frac{a^3}{E_i h_i} + \frac{b^3}{E_o h_o}\right) \tag{4}$$

where a and b are the mean radii of the inner and outer tubes, and the properties of these tubes are designated by subscripts i and o. Note that if the inner tube is made very small ($a \to 0$), then the original Korteweg-Joukowsky theory of (3) is recovered.

The predictions of this model are compared with experimental measurements in Fig. 4 and agree quite favorably, with errors less than 1-4%. The fact that the measured wave speeds are consistently lower than the predictions is due to small air bubbles in the water, which accumulate as the vessel is filled. These bubbles are difficult to eliminate since even a very small void fraction can significantly reduce wave speeds [16], though this effect is somewhat less significant for shock waves of finite strength [17].

Nonlinear Elastic Regime

Increasing the amplitude or duration of the pressure wave further results in excitation of elastic buckles. Pressure and strain measurements in this regime are shown in Fig. 5. In Fig. 5 (a) and (b), the response of a welded stainless steel tube (Tube

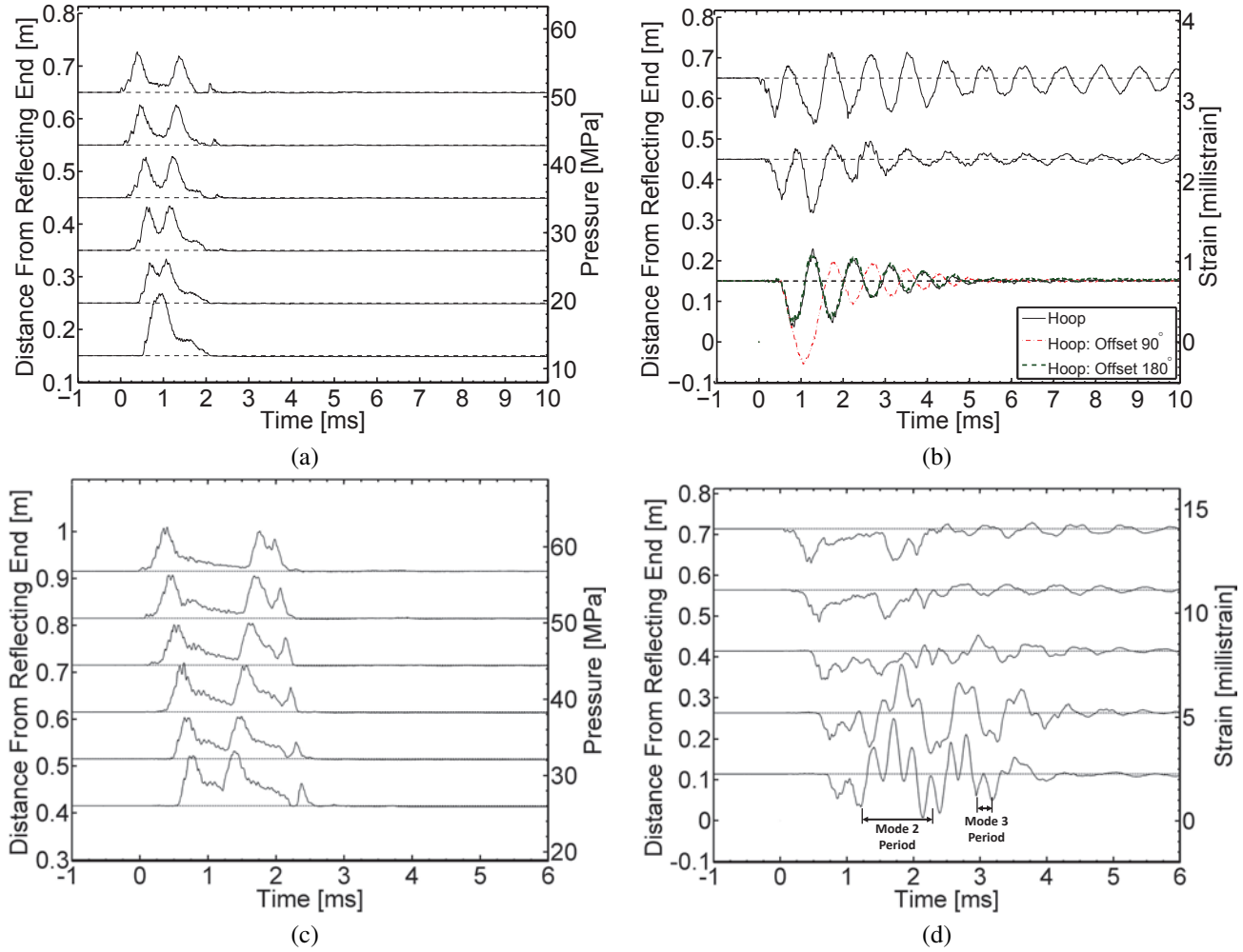

Fig. 5 (a) and (b): Pressure and hoop strain traces for Tube 54 showing mode 2 elastic vibrations. (c) and (d): Pressure and hoop strain traces for Tube 30 showing superposition of buckles in modes 2 and 3.

54) is shown. The tube develops a mode 2 buckle which remains elastic throughout the response, and when the pressure wave dies away the tube continues to vibrate in this mode 2 shape. The fact that the buckle consists of two lobes is confirmed by examining the three strain traces located 150 mm from the reflecting end of the tube. At this location, three hoop strain gauges were attached at three positions around the tube circumference: the first guage was located at the weld where a local minimum in wall thickness was measured, and the other two gauges were spaced in increments of 90°. For this tube, the buckle was aligned exactly with the weld (though this was not always the case for welded tubes) and the strain traces measured at the weld and 180° away are exactly in phase, while the strain trace between them is exactly out of phase. This indicates that the buckle is in a mode 2 shape.

In Fig. 5 (c) and (d), pressure and strain traces are shown for an aluminum tube (Tube 30) in which the peak pressure was about twice the static buckling pressure (3.7 MPa). In this case, elastic buckles of both modes 2 and 3 were simultaneously excited near the bottom end of the tube.

The frequencies of elastic vibration in modes 2 and 3 were extracted from the experimental strain traces using either a fast Fourier transform or by counting periods, depending on the number of cycles that were present in the data. To compare these measured frequencies with theoretical predictions, the tube was modeled using the shell equations of Sanders [18] which are appropriate for low circumferential wavenumbers n. The circumferential displacement v, radial displacement w, and pressure

Table 2 Comparison of predicted and measured vibration frequencies in modes 2 and 3. The corresponding dimensions and materials are available in Table 1.

Tube Number	Mode Number n	Predicted Frequency [kHz]	Measured Frequency [kHz]	Error [%]
30	2	1.28	1.24	3.0
30	3	4.05	3.97	2.0
34	2	0.53	0.54	2.4
34	3	1.76	1.85	4.7
36	2	1.75	1.82	3.8
43	2	1.28	1.20	6.4
46	2	0.86	0.85	1.2
46	3	2.84	2.82	0.7

p are taken to be harmonic vibrations of the following form:

$$\begin{aligned} \upsilon &= V \sin(n\theta)\cos(\omega t) \\ w &= W \cos(n\theta)\cos(\omega t) \\ p &= P \cos(n\theta)\cos(\omega)t \end{aligned} \tag{5}$$

in which case the equations of Sanders can be expressed as:

$$\begin{bmatrix} \Omega^2 - n^2(1+\alpha^2) & -n(1+\alpha^2 n^2) \\ n(1+\alpha^2 n^2) & 1+\alpha^2 n^4 - \Omega^2 \end{bmatrix} \begin{bmatrix} V \\ W \end{bmatrix} = -\frac{Pa^2(1-\nu^2)}{Eh} \begin{bmatrix} 0 \\ 1 \end{bmatrix} \tag{6}$$

where $\alpha^2 = h^2/12a^2$ is the shell parameter and Ω is the ratio of the frequency ω to the natural frequency of axisymmetric vibration:

$$\Omega \equiv \omega \sqrt{\frac{\rho a^2(1-\nu^2)}{E}} \tag{7}$$

The annulus of fluid was modeled using the linear wave equation for the velocity potential ϕ:

$$\frac{1}{c^2}\frac{\partial^2\phi}{\partial t^2} = \frac{\partial^2\phi}{\partial r^2} + \frac{1}{r}\frac{\partial\phi}{\partial r} + \frac{1}{r^2}\frac{\partial^2\phi}{\partial\theta^2} \tag{8}$$

which is subject to velocity boundary conditions at the inner ($r = a$) and outer ($r = b$) surfaces of the fluid annulus:

$$\left.\frac{\partial\phi}{\partial r}\right|_{r=a} = \frac{\partial w}{\partial t} \qquad\qquad \left.\frac{\partial\phi}{\partial r}\right|_{r=b} = 0 \tag{9}$$

The velocity potential ϕ is assumed to be of the form:

$$\phi(r,\theta,t) = \Phi(r)\cos(n\theta)\cos(\omega t) \tag{10}$$

Using using standard techniques from the theory of acoustics [19], the pressure at the surface of the specimen tube ($r = a$) is found to be:

$$P = \rho_w \omega^2 W \left[\frac{J_n(\gamma a)Y_n'(\gamma b) - J_n'(\gamma b)Y_n(\gamma a)}{J_n'(\gamma a)Y_n'(\gamma b) - J_n'(\gamma b)Y_n'(\gamma a)}\right] \tag{11}$$

where J_n and Y_n are n$^{\text{th}}$ order Bessel functions of the first and second kind and $\gamma = \omega/c$ is the radial wavenumber. Equations (6) and (11) constitute an eigenvalue problem for the frequency ω of vibration which can be solved numerically. The procedure used to derive Eqs. (6) and (11) and solve for the eigenvalues follows closely that of Warburton [20], who studied the vibration of tubes either containing a liquid or submerged in an infinite medium. The present analysis extends that method by considering an annulus of fluid and using shell equations which are better suited for low circumferential wavenumbers. Table 2 compares the experimentally measured frequencies of vibration in modes 2 and 3 with the lowest eigen-frequency from this model, and good agreement is found.

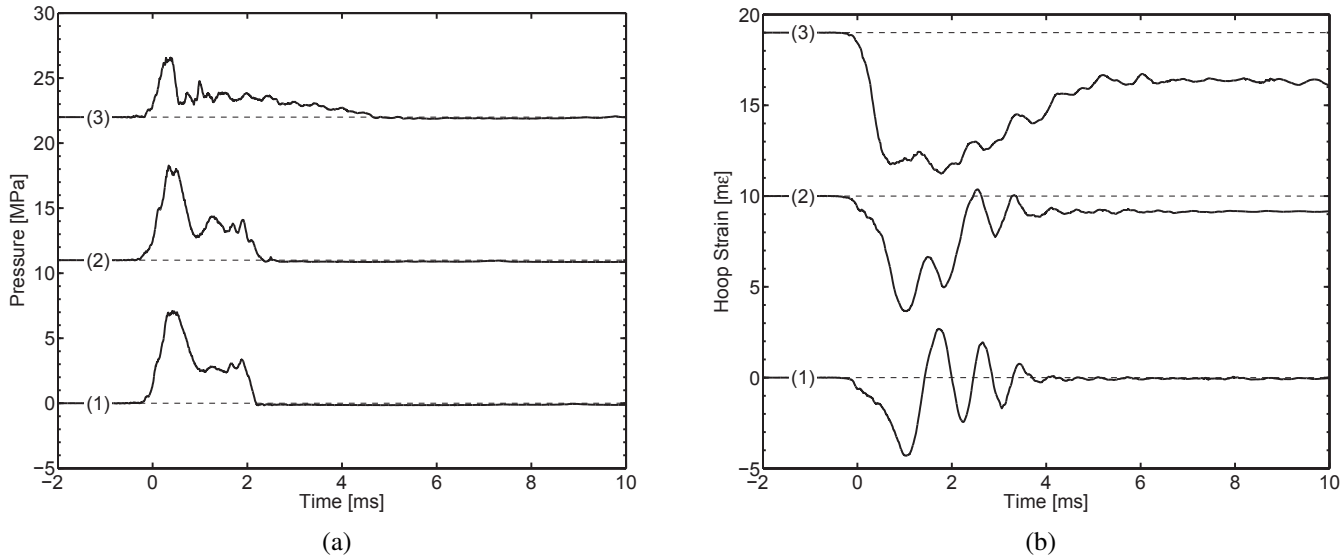

(a) (b)

Fig. 6 Pressure (a) and strain (b) traces for three consecutive shots using Tube 52 in which the pressure was gradually increased from shot to shot. Strain data was recorded 0.25 mm from the reflecting end of the tube, while pressure data was recorded at 0.15 m. Pressure and strain traces have been offset vertically for clarity.

Slightly Plastic Regime

To investigate the behavior very close to the onset of plastic deformation, a single tube was subjected to successive shots of gradually increasing pressure until plastic deformation first occurred. Pressure and strain traces from this shot sequence are shown in Fig. 6.

In the first shot, marked (1), mode 2 vibrations were excited but remained purely elastic with a peak measured strain of 4.3 millistrain, which is slightly below the yield value of about 4.5 millistrain for 6061-T6 aluminum. In the second shot (2), the peak measured strain was 6.3 millistrain and slight plastic deformation occurred, as evidenced by the final strain offset at the end of the trace. This offset is the result of residual stresses that are produced when the tube returns to its unloaded configuration after experiencing plastic deformation. It is worth noting that the pressure wave remains unchanged despite the occurrence of plastic deformation; however, the buckle grew slowly enough that plastic deformation did not occur until long after the arrival of the incident shock wave.

In the third shot (3), the peak strain was about 7.7 millistrain and further plastic deformation occurred. In this case, the peak measured pressure dropped by about 40% relative to shot (2), despite a 5% increase in the velocity of the projectile from the gas gun. Furthermore, the pressure wave dispersed considerably and decayed more slowly over time than in previous shots, indicating a strong interaction between the shock wave and the buckle. In spite of the considerable reduction in peak pressure, substantial plastic deformation was produced which demonstrates the reduction in the strength of the tube upon incidence of plastic deformation.

The progression of peak strains across the elastic and plastic regimes described above can be illustrated by plotting the peak measured strain against the peak measured pressure, as shown in Fig. 7. For low pressures, the peak strain is close to the static value given by:

$$\epsilon_{static} = \frac{pa(1-\nu^2)}{Eh} \tag{12}$$

At about the static buckling threshold (in this case, 3.67 MPa) the strain begins to deviate from the linear trend, but this deviation initially remains small since the buckles do not grow rapidly enough to be come significant during the short load duration. However, the peak strain appears to grow exponentially with pressure, so eventually large increases in strain are observed which bring the tube into the plastic range. In Fig. 7, the numbered points correspond to the strain traces shown in Fig. 6, where the onset of plastic deformation was examined. As shown at point (3), plastic deformation of the tube results in a considerable reduction of the peak pressure. However, the reduction in pressure and dispersion of the pressure wave may not be entirely due to deformation generated during shot (3), but may also involve the plastic deformation that remains from the preceding shot (2).

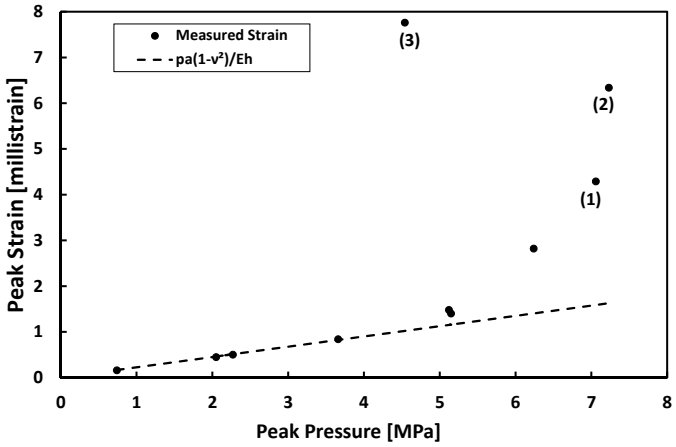

Fig. 7 Progression of peak strains as peak pressure is increased for Tube 52. Static buckling pressure is 3.67 MPa. Numbers in parenthesis correspond to the strain traces shown in Fig. 6.

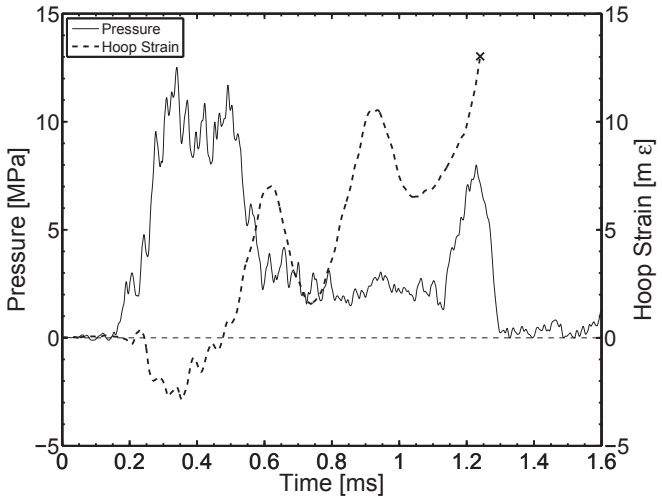

Fig. 8 Pressure and strain traces for a collapsing tube (Tube 43) with a static buckling pressure of 3.7 MPa. Pressure and strain were measured 150 mm from the top end of the specimen tube. The strain gauge de-bonded from the surface of the tube at the point marked by an **x**.

Collapse

The final regime of motion considered is that of pressures much greater than the buckling threshold. Examples of pressure and strain traces are shown in Fig. 8. The strain trace exhibits a sequence of vibrations superimposed over an offset that increases with time. Based on the frequency of these vibrations and the 3-lobed shape of the tube after collapse (shown in Fig. 9), these are interpreted as mode 3 vibrations. Even at this high pressure, the buckle appears to grow on a time-scale that is slow compared to motion of the pressure wave. For instance, the leading edge of the pressure wave has traveled nearly 0.5 m away from this location by the time the yield strain (about 4.5 millistrain) is first reached. This suggests that the incident pressure wave is not strongly affected by the development of buckles. However the reflected pressure wave, which arrives at about 1.2 ms, interacts with the buckle and its amplitude is reduced considerably.

Post-collapse photographs of tubes buckled in modes 2 and 3 are shown in Fig. 9. In the top pair of photographs, the thickest and thinnest points along the tube wall are indicated and the buckle is seen to align with these points. For extruded tubes, which featured sinusoidal wall-thickness variations around the circumference, alignment of the buckle with the points of maximum and minimum wall thickness was always observed for mode 2 buckles, indicating that this type of imperfection plays the dominant role in determining the orientation of the buckle. For mode 3 buckles, no clear trend was observed regarding the orientation of the buckle relative to the tube's wall thickness variations.

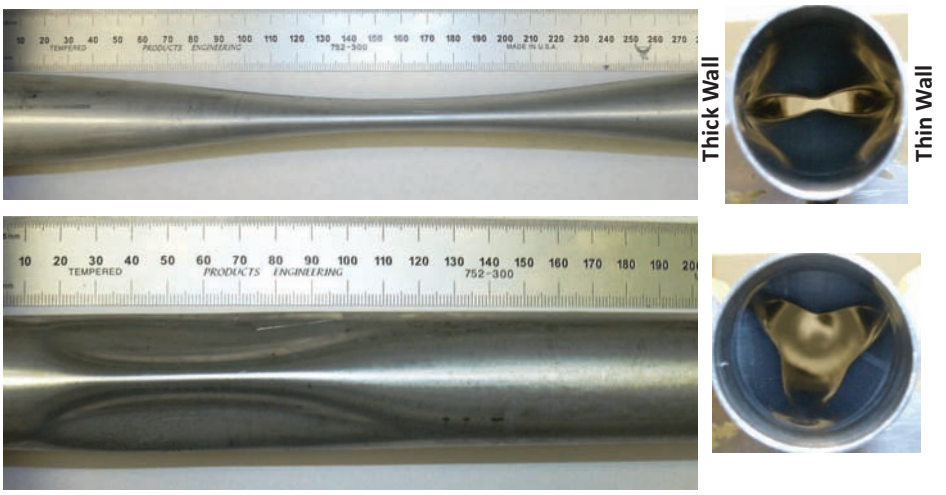

Fig. 9 Post-collapse photographs of Tube 37 (top) and Tube 43 (bottom) buckled in modes 2 and 3. The bottom photographs were taken following the test which generated the data plotted in Fig. 8. The thickest and thinnest points on the tube wall of the top photograph are indicated, demonstrating the alignment of the buckle with these points.

As shown in Fig. 9, the length of mode 2 buckles (about 8-10 tube diameters) is much longer than the length of mode 3 buckles (3-4 tube diameters). For a given mode number, these ratios of buckle length to tube diameter did not change significantly as the pressure was increased or the tube diameter changed.

Measurements of the Buckling Threshold

To make measurements of the buckling threshold, multiple shots were conducted on a single tube while gradually raising the peak pressure by increasing the projectile velocity from the gas gun. This was done until plastic deformation was first reached, at which point the tube was considered to be buckled. Each shot was characterized by its peak pressure and impulse, where the impulse was computed by integrating the pressure trace over the first 15 ms of data. The point at which buckling occurred can then be represented on a plot of pressure vs. impulse.

The results of this approach are shown in Fig. 10 for tubes with $a/h = 24.5$. Each line of data points represents a sequence of consecutive shots in which the projectile velocity from the gas gun was gradually increased, and the points marked by a black **x** mark the onset of plastic deformation, and hence represent points on the buckling threshold. As shown in the figure, the peak pressure and impulse increase in proportion to one another, which is expected since the apparatus operates at an approximately fixed load duration which is governed by the wave mechanics in the projectile and buffer.

One way to control ratio of peak pressure to peak impulse (i.e., the slope on the pressure-impulse diagram) is to change the lengths or materials of the buffer and projectile (see Fig. 1). For Tube 47 in Fig. 10 the usual aluminum buffer was used which was employed in all prior results presented in this paper. However, to obtain the data for Tube 50, a steel buffer was used instead, which reduced the slope on the pressure-impulse diagram and allowed a second point on the buckling threshold to be found. A third point on the buckling threshold was found using Tube 32 and an even smaller slope was achieved by making measurements in an alternate test apparatus which is very similar to that shown in Fig. 1, but features windows for visualizing the buckling process. The compliance of these windows reduces the speed of the pressure waves and increases the impulse for a given peak pressure.

The three tubes tested in Fig. 10 were identical, so differences in the peak pressure at which buckling occurred are caused only by the change in impulse of the pressure wave. For the shortest impulse tested, the peak pressure required to buckle the tube was about 7 times the static buckling threshold, which highlights the importance of inertial effects. The trend observed in these results agrees with the theoretical predictions of [7], which show that for large impulses the dynamic buckling threshold tends towards the static buckling pressure (1.3 MPa in this case), while for small impulses the threshold approaches a vertical asymptote at a particular critical impulse. In ref. [7], the following semi-empirical estimate of the critical impulse is suggested:

$$I_{cr} = 1.15\sqrt{\rho E}\frac{h^2}{a} \tag{13}$$

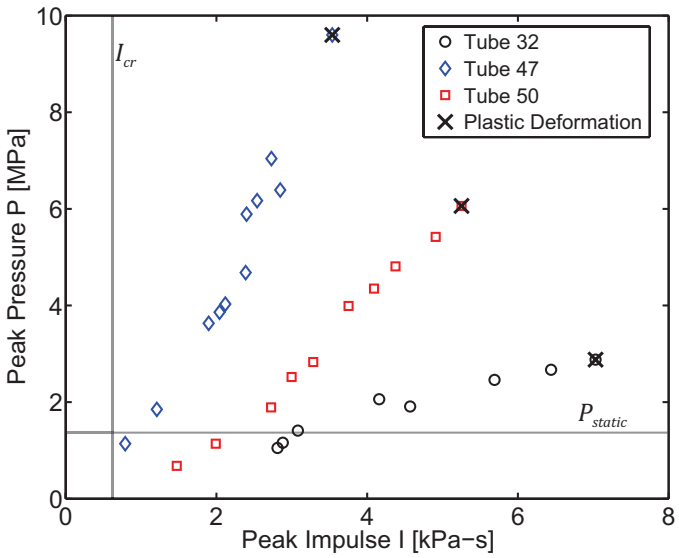

Fig. 10 Pressure vs. impulse curves for three identical aluminum tubes with radius a = 22 mm and a/h = 24.5. The static buckling threshold for these tubes is 1.3 MPa. Tube 47 was tested with an aluminum buffer, Tube 50 with a steel buffer, and Tube 32 in an alternate apparatus, allowing various regions of the pressure-impulse space to be reached. Black **x** marks points at which plastic deformation first occurred.

This formula predicts a critical impulse of about 0.57 kPa-s for the tubes in Fig. 10, though the effects of plasticity will become important as this limit is approached. This prediction is not inconsistent with the measurements shown in Fig. 10, but additional data points at lower impulses are needed to confirm that the buckling threshold approaches this asymptote.

Conclusions

Dynamic buckling of cylindrical tubes has been studied by submerging them in a thin annulus of water and generating axially-propagating shock waves in the water using a projectile impact facility. Measurements reveal that for low pressures, the response is similar to that of a waterhammer event occurring inside of a pipe, and suitably adapted waterhammer models are capable of adequately predicting the speed of the coupled fluid-solid waves. Elastic buckles are observed at higher pressures, but due to inertial effects these buckles do not fail the tube until the peak pressure is several times greater than the static buckling pressure. At that point, the onset of plastic deformation is found to substantially reduce the tubes' load-carrying capacity; however, it appears that plastic deformation does not significantly affect the motion of pressure waves since the leading edge of the pressure wave travels far from the buckle by the time plastic deformation is reached. Finally, these experiments have demonstrated that extruded tubes often feature sinusoidal wall thickness variations around the circumference, and these variations play a critical role in determining the orientation of mode 2 buckles.

Acknowledgements

This research was supported by the Office of Naval Research DOD MURI on Mechanics and Mechanisms of Impulse Loading, Damage and Failure of Marine Structures and Materials (ONR Grant No. N00014-06-1-0730), program manager Dr. Y. D. S. Rajapakse. Tomohiro Nishiyama of the Japan Patent Office and Prof. Kazuaki Inaba, currently at the Tokyo Institute of Technology, executed the initial design of the annular tube implosion fixture and supervised its fabrication while working at Caltech. Preliminary experiments on buckling using this facility were conducted by Mr. Jason Damazo and Dr. Rafal Porowski, currently at the research Center for Fire Protection in Poland. We are also grateful to Prof. Ravichandran of Caltech, who provided technical advice and leadership of the Caltech MURI.

References

[1] Lindberg, H. E., 1964. "Buckling of a very thin cylindrical shell due to an impulsive pressure". *Journal of Applied Mechanics,* ***31***, pp. 267–272.

[2] Abrahamson, G., Florence, A., and Lindberg, H., 1966. Investigation of response of simplified ICBM-type structures to impulsive loading. Tech. Rep. AFWL-TR-65-136, Stanford Research Institute.

[3] Anderson, D., and Lindberg, H., 1968. "Dynamic pulse buckling of cylindrical shells under transient lateral pressures". *AIAA Journal,* ***6***(4), pp. 589–598.

[4] Lindberg, H., Anderson, D., Firth, R., and Parker, L., 1965. Response of reentry vehicle-type shells to blast loads. Tech. Rep. LMSC-B130200-VOL-4-C, Stanford Research Institute.

[5] Lindberg, H. E., and Firth, R. D., 1967. Structural response of spine vehicles, volume II: Simulation of transient surface loads by explosive blast waves. Tech. Rep. AFWL-TR-66-163, Vol. II, Stanford Research Institute.

[6] Lindberg, H. E., and Sliter, G. E., 1969. Response of reentry-vehicle-type shells to transient surface pressures. Tech. Rep. AFWL-TR-68-56, Stanford Research Institute.

[7] Lindberg, H., and Florence, A., 1987. *Dynamic Pulse Buckling*. Martinus Nijhoff Publishers.

[8] Lindberg, H. E., 1974. "Stress amplification in a ring caused by dynamic instability". *Journal of Applied Mechanics,* ***41***, pp. 392–400.

[9] Inaba, K., and Shepherd, J. E., 2010. "Flexural waves in fluid-filled tubes subject to axial impact". *J. Pressure Vessel Technol.,* ***132***, April, p. 021302.

[10] Hutchinson, J., and Koiter, W., 1970. "Postbuckling theory". *Applied Mechanics Reviews,* ***23***(12), pp. 1353–1366.

[11] Kempner, J., Pandalai, K., Patel, S., and Crouzet-Pascal, J., 1957. "Postbuckling behavior of circular cylindrical shells under hydrostatic pressure". *Journal of the Aeronautical Sciences,* ***24***, pp. 253–264.

[12] Timoshenko, S. P., and Gere, J. M., 1961. *Theory of Elastic Stability*, 2nd ed. McGraw-Hill.

[13] Korteweg, D., 1878. "Über die fortphlanzungsgeschwindigkeit des schalles in elastisches röhren (on the velocity of propagation of sound in elastic pipes)". *Annalen der Physik und Chemie,* ***9***(5), pp. 525–542.

[14] Joukowsky, N., 1900. "Über den hydraulishen stoss in wasserleitungsröhren (on the hydraulic hammer in water supply pipes)". *Mémoires de l'Académie Impériale des Sciences de St. Péterbourg,* ***9***(5). Series 8.

[15] Shepherd, J. E., and Inaba, K., 2010. "Shock loading and failure of fluid-filled tubular structures". In *Dynamic Failure of Materials and Structures*, A. Shukla, G. Ravichandran, and Y. Rajapakse, eds. Springer, pp. 153–190.

[16] Wood, A. B., 1955. *A Textbook Of Sound*, third ed. G. Bell And Sons.

[17] Ando, K., Sandada, T., Inaba, K., Damazo, J., Shepherd, J. E., Colonius, T., and Brennen, C. E., 2011. "Shock propagation through a bubbly liquid in a deformable tube". *Journal of Fluid Mechanics,* ***671***, pp. 339–363.

[18] Leissa, A. W., 1973. Vibration of shells. Tech. Rep. NASA SP-288, National Aeronautics and Space Administration.

[19] Junger, M. C., and Feit, D., 1972. *Sound, Structures, and their Interaction*, second ed. MIT Press.

[20] Warburton, G., 1961. "Vibration of a cylindrical shell in an acoustic medium". *Journal of Mechanical Engineering Science,* ***3***(1), pp. 69–79.